AGU100 ADVANCING EARTH AND SPACE SCIENCE

Geophysical Research Letters

RESEARCH LETTER
10.1029/2018GL077472

Key Points:
- Generic models show that maximum cumulative stress change from earthquake interactions is comparable to pore pressure change from injection
- Earthquake interactions may be a triggering mechanism for injection-induced earthquakes
- Mitigation decisions may need to consider earthquake interactions to be effective

Supporting Information:
- Supporting Information S1
- Data Set S1
- Data Set S2
- Data Set S3

Correspondence to:
M. R. M. Brown,
megan.r.brown@colorado.edu

Citation:
Brown, M. R. M., & Ge, S. (2018). Small earthquakes matter in injection-induced seismicity. *Geophysical Research Letters*, *45*. https://doi.org/10.1029/2018GL077472

Received 6 FEB 2018
Accepted 24 MAY 2018
Accepted article online 4 JUN 2018

Small Earthquakes Matter in Injection-Induced Seismicity

Megan R. M. Brown[1] **and Shemin Ge**[1]

[1]Department of Geological Sciences, University of Colorado Boulder, Boulder, CO, USA

Abstract A simplistic triggering mechanism, pore pressure increase from injection, has been the focus of injection-induced seismicity studies for decades. Research into other possible mechanisms, like poroelastic stress changes, is ongoing, but there has been relatively little focus on earthquake interaction. While studies have looked at how moderate-magnitude events ($M \geq 3.0$) may trigger larger magnitude-induced seismicity, research into the cumulative effect of the hundreds to thousands of small-magnitude ($M \leq 3.0$) events is lacking. Here we use generic models to compare the possible stress changes from pore pressure increase and from earthquake interactions of small-magnitude events. We find that the area of increased pore pressure is much larger than that of positive Coulomb static stress transfer; however, maximum Coulomb static stress change is larger than maximum pore pressure increase. We argue that, yes, small earthquakes do matter, and their interaction may be an important triggering mechanism to consider.

Plain Language Summary Studies of the triggering mechanisms of injection-induced earthquakes have been investigated for decades, but the focus has been on the direct influence of fluid injection in causing fault failure. There have been limited studies into the role of earthquake interactions between the small-magnitude-induced seismicity even though there is evidence of earthquake interactions in natural earthquake sequences. In this study, we use models of idealized situations to compare the relative importance of the triggering mechanism of pore pressure change from injection and the triggering mechanism of earthquake interactions. We argue that the small induced earthquakes do matter and that earthquake interactions could have serious implications on the required timing of mitigation action.

1. Introduction

The basic physics of injection-induced seismicity has been understood for decades. In a nutshell, injected fluids increase pore pressure and decrease the effective stress on a critically stressed fault (Healy et al., 1968; Hubbert & Rubey, 1959), leading to fault failure and earthquakes. However, this is a very simplified view of the triggering mechanism. Coulomb static stress transfer, the process of slip along a fault causing static (permanent) stress change (King et al., 1994), has been used to describe earthquake interactions in a number of natural systems (e.g., King et al., 1994; Lin & Stein, 2004; Toda et al., 2005, 2011). The idea of earthquake interactions is that earthquake slip causes stress to change around the slip and this stress change causes further earthquakes (King et al., 1994). In natural systems, King et al. (1994) found that stress changes as low as 0.01 MPa can trigger seismicity.

Cumulative Coulomb static stress transfer can result from many small to moderate earthquakes. Ziv and Rubin (2000) calculated the cumulative static stress change in central California between 1969 and 1998 and found that cumulative static stress changes of much less than 0.01 MPa can still have a triggering effect. This is in line with the notion of a critically stressed crust (Townend & Zoback, 2000), which states that faults in the Earth's crust are at frictional equilibrium and only a small perturbation of stress will trigger failure. In the central United States and other areas, induced seismicity from wastewater injection has triggered hundreds to thousands of earthquakes (e.g., Ellsworth, 2013; Nakai et al., 2017; Weingarten et al., 2015). So in terms of triggering mechanisms, we ask the question: *What about the earthquakes?*

Studies have shown the Coulomb static stress change (ΔCSS) for a single or a few moderate-magnitude-induced seismic events (e.g., Chen et al., 2017; McNamara et al., 2015; Sumy et al., 2014). Sumy et al. (2014) argued that a moderate injection-induced earthquake, magnitude M5.0, led to the triggering of the M5.7 Prague, Oklahoma, earthquake through a series of earthquake interactions. Chen et al. (2017) calculated the ΔCSS from $M \geq 3.0$ earthquakes and suggest that the M5.8 Pawnee, Oklahoma, earthquake was also triggered by a combination of injection and earthquake interaction. However, the effects of *cumulative* ΔCSS from *small*-magnitude injection-induced seismicity ($M \leq 3.0$) have not been thoroughly investigated.

Helmstetter et al. (2005) estimated the relative importance of small and large earthquakes for static stress transfer and found that while large earthquakes matter more in terms of energy release, small earthquakes are just as important as larger earthquakes for stress changes. A large-magnitude event transfers more stress than a smaller one. However, the larger number of small earthquakes adds up. Cumulative static stress change of many small-magnitude events is comparable to static stress change of one large-magnitude event. Few studies have modeled ΔCSS caused by static stress transfer of actual induced seismicity. In one study, Catalli et al. (2013) modeled ΔCSS caused by microseismicity induced at the Basel Enhanced Geothermal site without considering stress changes caused by fluid injection. They found that 75% of the events occurred in areas of positive ΔCSS that promotes failure. The fact that the majority of earthquakes occur in those areas suggests that earthquake interaction may control subsequent earthquake locations and therefore is an important component of induced seismicity.

Coulomb static stress transfer has been discussed as a potential mechanism in wastewater injection-induced seismicity as well. Schoenball et al. (2018) investigated the Guthrie-Langston, Oklahoma, earthquakes and found some areas with continuous seismic activity and others with short bursts of seismic activity. They suggested that this could be due to two separate triggering mechanisms: slower pore pressure diffusion and more immediate static stress transfer. Further, based on analysis of spatiotemporal evolution of induced seismicity in Oklahoma and Southern Kansas, Schoenball and Ellsworth (2017) concluded that static stress transfer must play a role as a triggering mechanism. They point out that static stress transfer has a short range of influence and therefore could appear similar to fluid diffusion processes.

We hypothesize that pore pressure increase from wastewater injection promotes failure on critically stressed, optimally oriented faults (Figure 1) in areas where induced seismicity occurs. Initial earthquakes then promote further failure through Coulomb static stress transfer. This process of earthquake interactions may continue and promote failure beyond the area of pore pressure increase, after injection has reduced rates or ceased entirely, and/or at larger magnitudes than previous events (Figure 1b). By convention, positive ΔCSS (designated by warm colors) indicates stress change that brings areas closer to failure while negative ΔCSS (designated by cool colors) stabilizes areas. In addition, there may be a "mitigation limit" for mitigation action of the injection parameters (e.g., injection rate and injection well spacing) if earthquake interactions become an equal or dominate triggering mechanism for the induced seismicity (Figure 1b). If that scenario occurs, mitigation of the seismicity may be ineffective and earthquakes will continue until the system returns to equilibrium. The objective of this study is to compare the relative importance of pore pressure increase and earthquake interactions as triggering mechanisms for injection-induced seismicity.

2. Methods

Here we use two generic models: one modeling pore pressure change from wastewater injection (Figure S1a) and the other modeling Coulomb static stress transfer from a single cluster of earthquakes on two idealized faults (Figure S1b). The models are independent of one another, and the stress changes are compared as separate but complementary triggering mechanisms. We use independent models to compare the stress change caused by reasonable scenarios of injection and earthquake occurrence to determine if the cumulative effect of small-magnitude earthquakes can generate the same level of stress change as pore pressure increase that initiates the induced seismicity.

2.1. Pore Pressure Modeling

We model pore pressure change (ΔP) using a model with one injection well in the center of the model domain. The 3D model dimension is 50 km by 50 km by 10 km. A cross-sectional view of the model domain through the injection well is shown in Figure S1a. The model consists of three lithologic layers: a 1,000-m-thick confining layer starting at the surface (0 to −1,000 m), a 500-m-thick injection interval (−1,000 to −1,500 m), and 8,500 m of crystalline basement (−1,500 to −10,000 m). We use MODFLOW-2005 to model ΔP caused by injection (full details in Text S1). We conduct numerous simulations using reasonable ranges of values for permeability, specific storage, and injection rate. We vary permeability of the injection interval between 10^{-16} and 10^{-12} m^2. The crystalline basement has the same permeability of the injection interval at the contact and decreases with depth to 10^{-18} m^2 at −10,000 m. We vary specific storage between 10^{-7} and 10^{-5} m^{-1}. We run the models varying injection rates between 2,000 and 4,240 m^3/day (~377,400 and

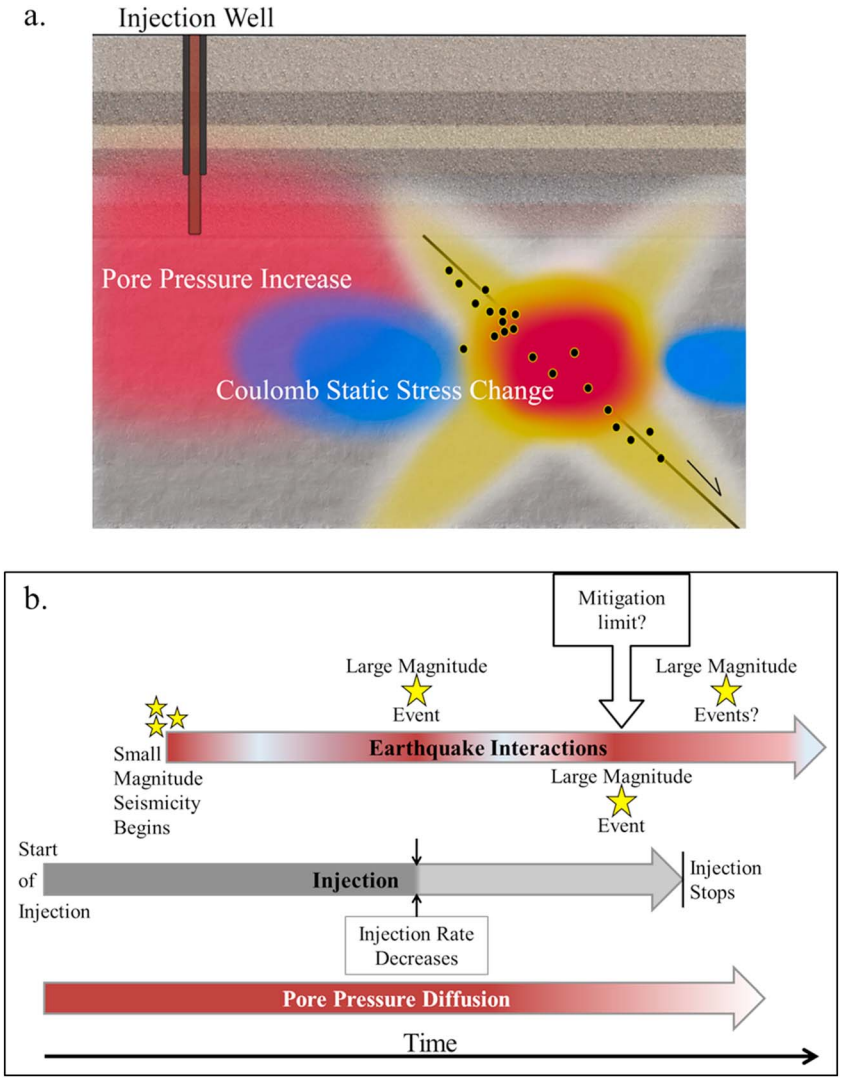

Figure 1. Conceptual interpretation of physical triggering mechanisms. (a) Conceptual cross-section diagram (perpendicular to normal fault strike) showing stress changes caused by possible triggering mechanisms. The warm colors (yellows to reds) represent positive stress change that promotes failure, and the cool colors (blues) represent negative stress change that promotes stability. The black dots represent hypothetical earthquakes in the crystalline basement below the injection interval. (b) Hypothesized scenario of triggering mechanisms, and the relationship to injection and mitigation actions.

~800,000 barrels per month). Each simulation models ΔP due to injection at a constant rate for 10 years. A full summary of model parameters for each simulation is included in Table S1.

2.2. Coulomb Static Stress Transfer Modeling

Coulomb static stress transfer modeling was conducted using U.S. Geological Survey Coulomb 3 software (Lin & Stein, 2004; Toda et al., 2005), which calculates static stress transfer in an elastic half-space with uniform isotropic elastic properties. Coulomb static stress transfer is the process whereby static stress change results from slip along a source fault. Coulomb static stress transfer can promote or reduce the potential for earthquake triggering (e.g., King et al., 1994; Stein, 1999, 2005; Toda et al., 2012) based on the change of shear and normal stresses on the fault. After an earthquake, ΔCSS can be calculated on faults in areas around the earthquake slip, particularly receiver faults or optimally oriented faults. Receiver faults are faults with prescribed orientations; optimally oriented faults are faults with orientations

most prone to slip in a given background stress. Coulomb static stress change (ΔCSS) is calculated as (Stein, 1999)

$$\Delta\mathrm{CSS} = \Delta\tau_s + \mu'(\Delta\sigma_n) \quad (1)$$

where $\Delta\tau_s$ is shear stress change (positive when increased in the direction of fault slip), μ' is effective coefficient of fault friction on the receiver fault, and $\Delta\sigma_n$ is normal stress change (positive when the fault is unclamped). Calculating static stress transfer to a prescribed fault orientation, receiver fault, is independent of background stress, but relies on the coefficient of friction, fault geometry, and sense of slip (King et al., 1994).

We examine two idealized fault scenarios in this study (Figure S1b): (1) a vertical left-lateral strike-slip fault and (2) a normal fault striking 0° north and dipping 60° east. We generate the earthquake catalogs used to calculate Coulomb static stress transfer using the Gutenberg-Richter (Gutenberg & Richter, 1944) magnitude-frequency relation, which is the power law:

$$\log_{10}N = a - bM, \quad (2)$$

where N is the number of events greater than or equal to magnitude M and a and b are constants. The constant b relates the frequency of small events to larger events—the larger the b-value, the more small-magnitude events there are in relation to large-magnitude events. The constant a relates to the productivity or total number of events for the system. We use three b-values low, average, and high (0.8, 1.0, and 1.2, respectively) and keep a consistent at $a = 3$. A range of b-values has been calculated for induced seismicity from low ($<$1.0) b-values (Goebel et al., 2017) to high ($>$1.0) b-values (e.g., Bachmann et al., 2012; Brown & Liu, 2016; Goebel et al., 2017; Mousavi et al., 2017; Ogwari et al., 2018). We include all earthquakes of magnitude 1.0 and larger. The generated catalogs (Data Set S1) are 158 events with magnitudes from M1.0 to M3.7 for $b = 0.8$, 100 events with magnitudes from M1.0 to M3.0 for $b = 1.0$, and 63 events with magnitudes from M1.0 to M2.5 for $b = 1.2$. We assigned random locations to each of the events using statistical distributions normalized to fault size (Mai et al., 2005) and realistic fault sizes (Text S2). We chose a fault length of 10 km and fault width of 4 km, which is consistent with fault sizes for induced seismicity in New Mexico (Nakai et al., 2017), Oklahoma (Yeck, Weingarten, et al., 2016; Yeck et al., 2017), and Arkansas (Horton, 2012).

In addition to earthquake locations, earthquake parameters were needed for each event. Earthquake parameters include rupture length, rupture width, average slip, and slip direction. Coulomb 3 has built-in empirical fault relationships between earthquake magnitude and earthquake parameters, derived by Wells and Coppersmith (1994). The empirical relationships, however, were derived based on earthquakes $M > 4.5$. Since the modeled seismicity is of $M \leq 3.7$ using Wells and Coppersmith (1994) is not appropriate. Therefore, we use alternative relations (Leonard, 2010) to determine fault rupture length, fault rupture width, and average displacement (Table S2). The relations developed by Leonard (2010) apply to faults of all lengths and magnitudes. The earthquake locations are taken as the center point of earthquake rupture. We use parameters calculated from the relations of Leonard (2010) and set rupture length and rupture width around the center points. We set the slip direction to be pure left-lateral strike-slip faulting or pure downdip normal faulting. We use an effective coefficient of friction of 0.6 and Young's modulus of 80 GPa. We simulate the slip of each event as a rupture along a single fault. We calculate Coulomb static stress transfer for the cumulative change from all events for each catalog. The stress change is calculated on a receiver fault of the same orientation and slip direction as the source fault with the modeled earthquakes. The intention is to determine stress changes along the fault with sections that are already activated. In addition, we modeled scenarios with variable focal mechanisms (Text S2) for a more realistic faulting scenario along a single fault.

3. Results

3.1. Pore Pressure Modeling Results

Results from pore pressure modeling show that pore pressure increase varies over several orders of magnitude with changing parameters. The results shown in Figure 2a are ΔP directly below the injection well within the crystalline basement. We eliminated two model simulations due to unrealistically high pressures near the

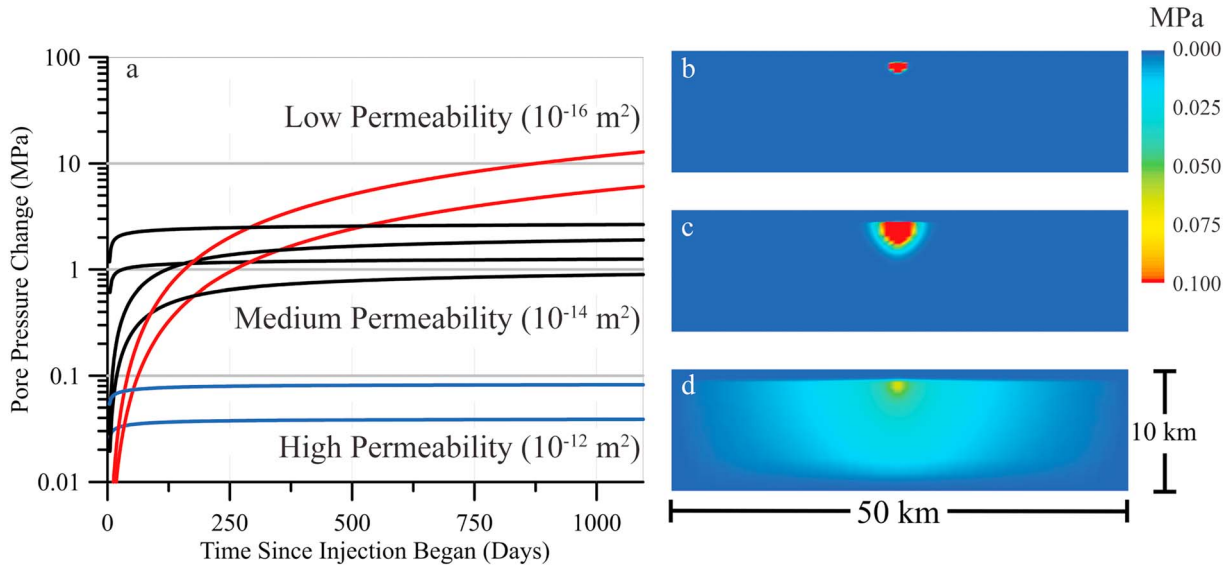

Figure 2. Pore pressure modeling results. (a) Graph of ΔP at the yellow dot, shown in Figure S1a, directly below the injection well in crystalline basement. Simulations are grouped by permeability of injection interval (low, medium, or high). (b–d) Cross sections of ΔP through the injection well after three years (1,095 days) of constant injection. (b) Low permeability, (c) medium permeability, and (d) high permeability.

injection well, but include them in Figure S2. Results are most sensitive to the hydraulic permeability of the injection interval and crystalline basement. Maximum ΔP varies from 0.04 to 42.6 MPa. This is consistent with other site-specific pore pressure models of induced seismicity (e.g., Brown et al., 2017; Healy et al., 1968; Hornbach et al., 2015; Keranen et al., 2014; Nakai et al., 2017; Ogwari et al., 2018; Ogwari & Horton, 2016). Low permeability generates the largest pore pressure increase, but pore pressure does not diffuse very far into the basement or laterally (Figure 2b); high permeability generates much further diffusion of pore pressure increase, but the magnitude of the increase is much smaller (Figure 2d) than low and medium permeability simulations (Figures 2b and 2c).

3.2. Coulomb Static Stress Modeling Results

Results of the Coulomb static stress transfer modeling show that the largest change in stress was in the lowest *b*-value scenarios, consistent with a larger number of events with higher magnitude (Figure 3). The ΔCSS is shown in Figure 3 for average depth of the earthquakes, ranging from 3.8 to 4.3 km (Table S3), and in the direction of slip of the source fault. There are areas of positive ΔCSS in all scenarios that are as large as or larger than estimated triggering thresholds of pore pressure (~0.07 to 0.10 MPa) from site-specific studies (e.g., Brown et al., 2017; Keranen et al., 2014). Maximum ΔCSS at average depth varies from approximately 12 to 770 MPa in strike-slip fault scenarios (Figures 3a–3c) and approximately 18 to 62 MPa in normal fault scenarios (Figures 3d–3f).

We also calculate modeled area at target depths (top of basement in ΔP models and average depth of earthquakes for ΔCSS models) with stress changes ≥0.01 and ≥ 0.10 MPa (Figures S3 and S4). Sensitivity analysis is conducted to determine the effect varying the effective coefficient of friction has on the model, and it is found that the maximum ΔCSS and modeled area is largely insensitive to the effective coefficient of friction (Table S5). Hardebeck (2006) found that for small fault lengths, focal mechanism variability is within one standard deviation uncertainty of focal mechanisms, ~25°. Focal mechanism studies of induced seismicity in Texas (Quinones et al., 2018) found that the mechanisms in single sequences are surprisingly consistent. Further sensitivity studies were conducted using variable focal mechanisms (Text S2). While varied focal mechanism scenarios resulted in a decreased maximum ΔCSS (Table S4) compared to consistent (pure strike slip or normal faulting) focal mechanism scenarios (Figure 4), the values are still as large as or larger than maximum ΔP. In addition, we modeled the ΔCSS for single moderate-magnitude events with a seismic moment similar to the cumulative moment of the small-magnitude events. Maximums of ΔCSS and most modeled areas above the stress threshold are lower than for the small-magnitude scenarios (Table S6).

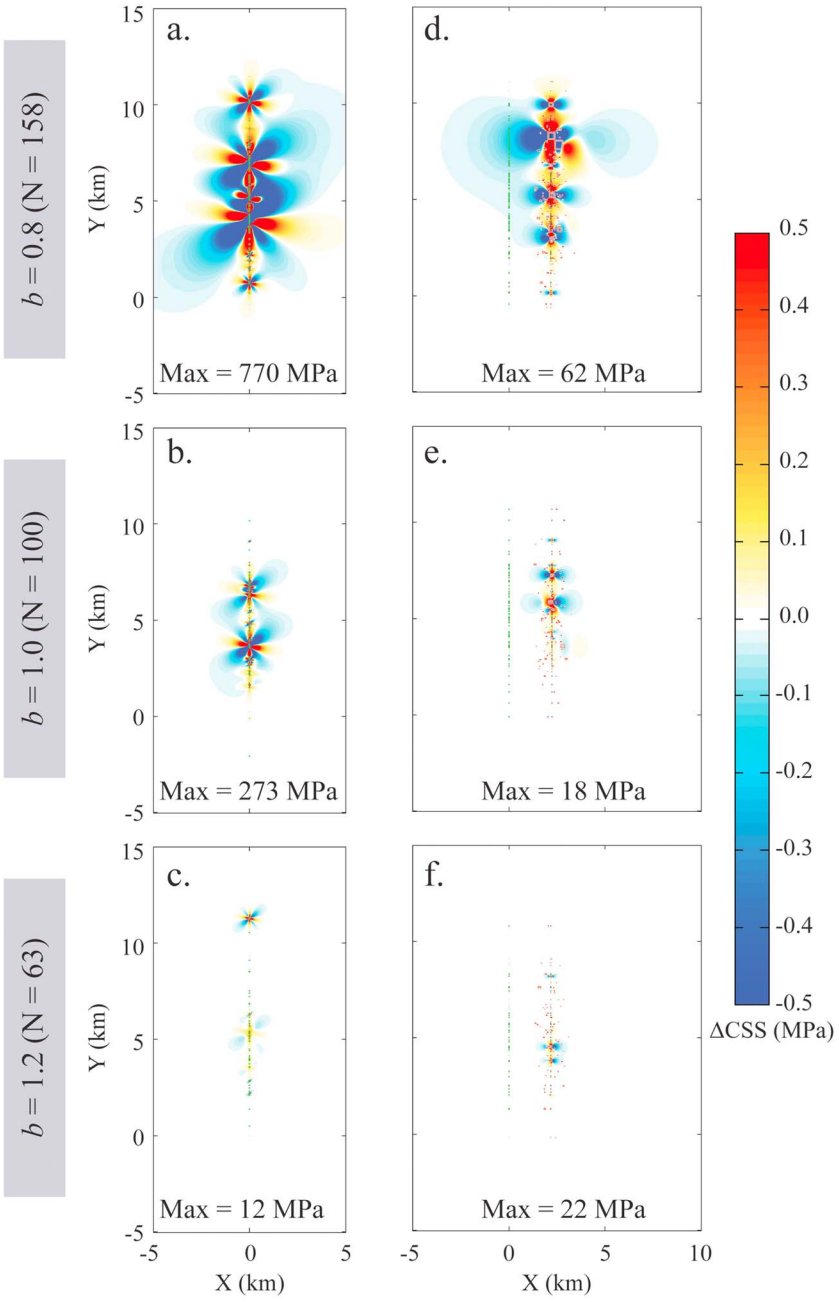

Figure 3. Coulomb static stress transfer model results for six event sequences at the average depth of the earthquakes for a receiver fault with the same orientation and direction of slip as the modeled earthquakes. (a–c) Left-lateral strike-slip fault results and (d–f) normal fault results. First row (a and d) is results for the catalog of 158 events generated using a *b*-value of 0.8; second row (b and e) is results for the catalog of 100 events generated using a *b*-value of 1.0; and third row (c and f) is results for the catalog of 63 events generated using a *b*-value of 1.2. The maximum positive ΔCSS is indicated for each scenario.

4. Discussion

We compare magnitude of maximum ΔP from pore pressure modeling and maximum ΔCSS from Coulomb static stress transfer modeling in Figure 4a. A 1:1 line is included to separate ΔP dominated and ΔCSS dominated regions. We find that in the majority of cases, maximum ΔCSS is larger than maximum ΔP. This comparison shows that after a sequence of small-magnitude events occurs, positive ΔCSS is at least

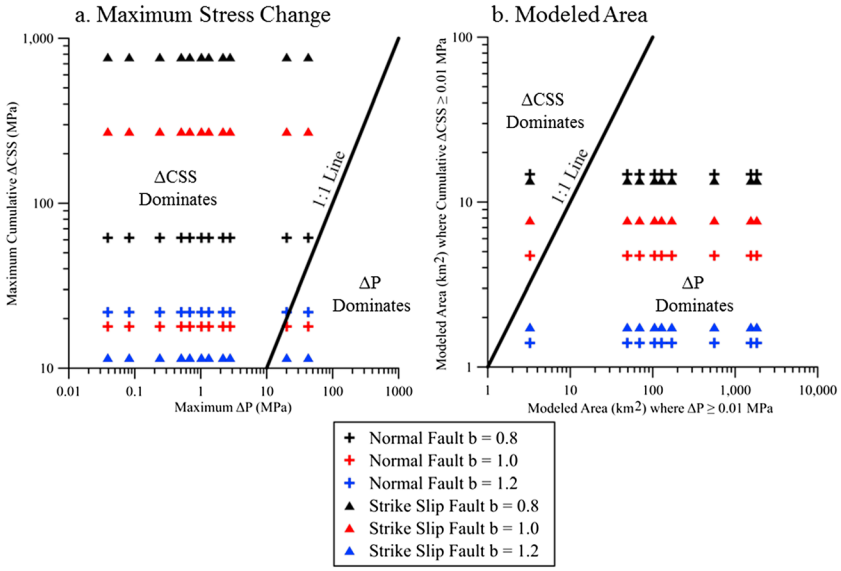

Figure 4. Comparison of modeled ΔP to modeled ΔCSS. The black lines indicate the 1:1 line separating the ΔCSS dominate region (above) from the ΔP dominate region (below). (a) Comparison of modeled maximum ΔP to modeled maximum ΔCSS. (b) Comparison of areas with modeled stress changes greater than or equal to 0.01 MPa. Area is calculated at average depth of the earthquakes for ΔCSS and directly below the injection interval at top of crystalline basement for ΔP.

comparable to the ΔP. Therefore, earthquake interactions between small-magnitude events initially induced by pore pressure increase may induce further seismicity in the same area.

We also compare the areas where modeled stress changes are ≥0.01 MPa (Figure 4b) for the average depth of the earthquakes (Table S3) for ΔCSS results and the top of crystalline basement directly below the injection interval for ΔP results. For the majority of the pore pressure model scenarios, the area of ΔP is larger than ΔCSS in the Coulomb static stress transfer models. This confirms the recognized importance of pore pressure increase in inducing seismicity. The larger spatial extent of pore pressure change above the threshold of 0.01 MPa elevates the potential for encountering critically stressed optimally oriented faults. However, the much larger maximum stress change seen in the Coulomb static stress transfer modeling illustrates the importance of ΔCSS triggering. While the area of modeled stress increase above the 0.01 MPa threshold is small, the area is near the activated fault. The earthquake interactions could induce additional earthquakes along the fault that other events have already occurred.

Results of this study indicate the possible significance earthquake interactions can have in guiding mitigation efforts for injection-induced seismicity. Injection-induced seismicity has caused no deaths in the United States, but has caused property damage (Morgan & Morgan, 2011; Yeck, Sheehan, et al., 2016), personal injury (Yeck et al., 2017), and increased risk of damaging critical infrastructure (McNamara et al., 2015). Earthquake interactions may provide urgency for mitigation actions if the stress transfer from earthquake interaction generates sufficient stress changes to encourage continued induced seismicity. If earthquakes are shown to promote further triggering of more earthquakes (Figure 1), then effective mitigation options may be limited by how many earthquakes occur prior to mitigation action being taken.

In addition, in some instances, the largest induced events have occurred following injection wells reducing or ceasing injection (e.g., Kim, 2013; Yeck et al., 2017). In both Youngstown, Ohio (Kim, 2013) and Fairview, Oklahoma (Yeck et al., 2017) cases, the largest magnitude events occurred following sequences of small-magnitude events. Continued seismicity could be related to pore pressure diffusion and/or earthquake interactions. Induced seismicity has been observed at great distances (e.g., Block et al., 2015; Keranen et al., 2014), 20–30 km or more, from the injection well. It may be possible that earthquake interactions of the small earthquakes near the largest events were a triggering mechanism for new earthquakes likely in addition to triggering by pore pressure increase. Finally, Coulomb static stress transfer has been indicated as a possible triggering mechanism for the two largest earthquakes in Oklahoma, the M5.7 Prague (Sumy et al., 2014) and

M5.8 Pawnee (Chen et al., 2017) events. Considering the role of earthquake interaction of small-magnitude events could be crucial to proper mitigation action decisions. Further site-specific studies are needed to determine the extent of Coulomb static stress transfer as a mechanism for injection-induced seismicity.

5. Conclusions

Our generic models show that Coulomb static stress transfer from small earthquakes ($1.0 \leq M \leq 3.7$) can have a cumulative effect that generates stress changes as large as or larger than the modeled ΔP caused by wastewater injection. Maximum ΔCSS ranged approximately 12–770 MPa in strike-slip fault scenarios and approximately 18–62 MPa in normal fault scenarios. Pore pressure increase in the generic groundwater model reached to as high as 42.6 MPa. Therefore, the stress changes that can promote seismicity are comparable for both triggering mechanisms, pore pressure increase from injection and earthquake interactions. However, the areas of increased pore pressure are much larger than the areas of positive ΔCSS, which means that there is a higher potential for pore pressure increased area to encounter additional critically stressed faults. The positive ΔCSS does remain close to the modeled fault and may promote additional slip along the activated fault. This work indicates that the role of the induced earthquake interactions, even though they are small-magnitude events, could generate more induced seismicity. The positive ΔCSS near the already activated fault may limit the effectiveness of mitigation by triggering more earthquakes.

Acknowledgments
We thank Gavin Hayes, Mirko van der Baan, and an anonymous reviewer for their helpful comments. Funding for this work was provided in part by USGS National Earthquake Hazards Reduction Program (NEHRP) grant G16AP00010. Data used in this study are included in the supporting information.

References

Bachmann, C. E., Wiemer, S., Goertz-Allmann, B. P., & Woessner, J. (2012). Influence of pore-pressure on the event-size distribution of induced earthquakes. *Geophysical Research Letters*, *39*, L09302. https://doi.org/10.1029/2012GL051480

Block, L. V., Wood, C. K., Yeck, W. L., & King, V. M. (2015). Induced seismicity constraints on subsurface geological structure, Paradox Valley, Colorado. *Geophysical Journal International*, *200*(2), 1172–1195. https://doi.org/10.1093/gji/ggu459

Brown, M. R. M., Ge, S., Sheehan, A. F., & Nakai, J. S. (2017). Evaluating the effectiveness of induced seismicity mitigation: Numerical modeling of wastewater injection near Greeley, Colorado. *Journal of Geophysical Research: Solid Earth*, *122*, 6569–6582. https://doi.org/10.1002/2017JB014456

Brown, M. R. M., & Liu, M. (2016). Injection-induced seismicity in Carbon and Emery Counties, central Utah. *Geofluids*, *16*(5), 801–812. https://doi.org/10.1111/gfl.12184

Catalli, F., Meier, M.-A., & Wiemer, S. (2013). The role of Coulomb stress changes for injection-induced seismicity: The Basel enhanced geothermal system. *Geophysical Research Letters*, *40*, 72–77. https://doi.org/10.1029/2012GL054147

Chen, X., Nakata, N., Pennington, C., Haffener, J., Chang, J. C., He, X., et al. (2017). The Pawnee earthquake as a result of the interplay among injection, faults and foreshocks. *Scientific Reports*, *7*(1), 4945. https://doi.org/10.1038/s41598-017-04992-z

Ellsworth, W. L. (2013). Injection-induced earthquakes. *Science*, *341*(6142), 1225942. https://doi.org/10.1126/science.1225942

Goebel, T. H. W., Weingarten, M., Chen, X., Haffener, J., & Brodsky, E. E. (2017). The 2016 Mw5.1 Fairview, Oklahoma earthquakes: Evidence for long-range poroelastic triggering at >40 km from fluid disposal wells. *Earth and Planetary Science Letters*, *472*, 50–61. https://doi.org/10.1016/j.epsl.2017.05.011

Gutenberg, B., & Richter, C. F. (1944). Frequency of earthquakes in California. *Bulletin of the Seismological Society of America*, *36*, 185–188.

Hardebeck, J. L. (2006). Homogeneity of small-scale earthquake faulting, stress, and fault strength. *Bulletin of the Seismological Society of America*, *96*(5), 1675–1688. https://doi.org/10.1785/0120050257

Healy, J. H., Rubey, W. W., Griggs, D. T., & Raleigh, C. B. (1968). The Denver earthquakes. *Science*, *161*(3848), 1301–1310. https://doi.org/10.1126/science.161.3848.1301

Helmstetter, A., Kagan, Y. Y., & Jackson, D. D. (2005). Importance of small earthquakes for stress transfers and earthquake triggering. *Journal of Geophysical Research*, *110*, B05S08. https://doi.org/10.1029/2004JB003286

Hornbach, M. J., DeShon, H. R., Ellsworth, W. L., Stump, B. W., Hayward, C., Frohlich, C., et al. (2015). Causal factors for seismicity near Azle, Texas. *Nature Communications*, *6*(1), 6728. https://doi.org/10.1038/ncomms7728

Horton, S. (2012). Disposal of hydrofracking waste fluid by injection into subsurface aquifers triggers earthquake swarm in Central Arkansas with potential for damaging earthquake. *Seismological Research Letters*, *83*(2), 250–260. https://doi.org/10.1785/gssrl.83.2.250

Hubbert, M. K., & Rubey, W. W. (1959). Role of fluid pressure in mechanics of overthrust faulting. *Geological Society of America Bulletin*, *70*(2), 115–206. https://doi.org/10.1130/0016-7606(1959)70[115:ROFPIM]2.0.CO;2

Keranen, K. M., Weingarten, M., Abers, G. A., Bekins, B. A., & Ge, S. (2014). Induced earthquakes. Sharp increase in central Oklahoma seismicity since 2008 induced by massive wastewater injection. *Science*, *345*(6195), 448–451. https://doi.org/10.1126/science.1255802

Kim, W.-Y. (2013). Induced seismicity associated with fluid injection into a deep well in Youngstown, Ohio. *Journal of Geophysical Research: Solid Earth*, *118*, 3506–3518. https://doi.org/10.1002/jgrb.50247

King, G. C. P., Stein, R. S., & Lin, J. (1994). Static stress changes and the triggering of earthquakes. *Bulletin of the Seismological Society of America*, *84*(3), 935–953.

Leonard, M. (2010). Earthquake fault scaling: Self-consistent relating of rupture length, width, average displacement, and moment release. *Bulletin of the Seismological Society of America*, *100*(5A), 1971–1988. https://doi.org/10.1785/0120090189

Lin, J., & Stein, R. S. (2004). Stress triggering in thrust and subduction earthquakes and stress interaction between the southern San Andreas and nearby thrust and strike-slip faults. *Journal of Geophysical Research: Solid Earth*, *109*, B02303. https://doi.org/10.1029/2003JB002607

Mai, P. M., Spudich, P., & Boatwright, J. (2005). Hypocenter locations in finite-source rupture models. *Bulletin of the Seismological Society of America*, *95*(3), 965–980. https://doi.org/10.1785/0120040111

McDonald, M. G., & Harbaugh, A. W. (1988). A modular three-dimensional finite-difference ground-water flow model. In US Geological Survey Techniques of Water-Resources Investigations (pp. 586).

McNamara, D. E., Hayes, G. P., Benz, H. M., Williams, R. A., McMahon, N. D., Aster, R. C., et al. (2015). Reactivated faulting near Cushing, Oklahoma: Increased potential for a triggered earthquake in an area of United States strategic infrastructure. *Geophysical Research Letters*, *42*, 8328–8332. https://doi.org/10.1002/2015GL064669

Morgan, M. L., & Morgan, K. S. (2011). Preliminary damage report of the August 22, 2011 Mw 5.3 earthquake near Trinidad, Colorado. Retrieved from http://coloradogeologicalsurvey.org/wp-content/uploads/2013/08/Preliminary-Damage-Report-of-the-Mw-5-3-Triniadad-Earthquake.pdf

Mousavi, S. M., Ogwari, P. O., Horton, S. P., & Langston, C. A. (2017). Spatio-temporal evolution of frequency-magnitude distribution and seismogenic index during initiation of induced seismicity at Guy-Greenbrier, Arkansas. *Physics of the Earth and Planetary Interiors*, *267*, 53–66. https://doi.org/10.1016/j.pepi.2017.04.005

Nakai, J. S., Weingarten, M., Sheehan, A. F., Bilek, S. L., & Ge, S. (2017). A possible causative mechanism of Raton Basin, New Mexico and Colorado earthquakes using recent seismicity patterns and pore pressure modeling. *Journal of Geophysical Research: Solid Earth*, *122*, 8051–8065. https://doi.org/10.1002/2017JB014415

Ogwari, P. O., DeShon, H. R., & Hornbach, M. J. (2018). The Dallas-Fort Worth airport earthquake sequence: Seismicity beyond injection period. *Journal of Geophysical Research: Solid Earth*, *123*, 553–563. https://doi.org/10.1002/2017JB015003

Ogwari, P. O., & Horton, S. P. (2016). Numerical model of pore-pressure diffusion associated with the initiation of the 2010-2011 Guy-Greenbrier, Arkansas earthquakes. *Geofluids*, *16*(5), 954–970. https://doi.org/10.1111/gfl.12198

Quinones, L. A., DeShon, H. R., Magnani, M. B., & Frohlich, C. (2018). Stress orientations in the Fort Worth Basin, Texas, determined from earthquake focal mechanisms. *Bulletin of the Seismological Society of America*, *108*(3A), 1124–1132. https://doi.org/10.1785/0120170337

Schoenball, M., & Ellsworth, W. L. (2017). A systematic assessment of the spatiotemporal evolution of fault activation through induced seismicity in Oklahoma and southern Kansas. *Journal of Geophysical Research: Solid Earth*, *122*, 10,189–10,206. https://doi.org/10.1002/2017JB014850

Schoenball, M., Walsh, F. R., Weingarten, M., & Ellsworth, W. L. (2018). How faults wake up: The Guthrie-Langston, Oklahoma earthquakes. *The Leading Edge*, *37*(2), 100–106. https://doi.org/10.1190/tle37020100.1

Stein, R. S. (1999). The role of stress transfer in earthquake occurrence. *Nature*, *402*(6762), 605–609. https://doi.org/10.1038/45144

Stein, R. S. (2005). Earthquake conversations. *Scientific American*, *15*(2), 82–89. https://doi.org/10.1038/scientificamerican0705-82sp

Sumy, D. F., Cochran, E. S., Keranen, K. M., Wei, M., & Abers, G. A. (2014). Observations of static Coulomb stress triggering of the November 2011M5.7 Oklahoma earthquake sequence. *Journal of Geophysical Research: Solid Earth*, *119*, 1904–1923. https://doi.org/10.1002/2013JB010612

Toda, S., Lin, J., & Stein, R. S. (2011). Using the 2011 Mw 9.0 off the Pacific coast of Tohoku earthquake to test the Coulomb stress triggering hypothesis and to calculate faults brought closer to failure. *Earth, Planets and Space*, *63*(7), 725–730. https://doi.org/10.5047/eps.2011.05.010

Toda, S., Stein, R. S., Beroza, G. C., & Marsan, D. (2012). Aftershocks halted by static stress shadows. *Nature Geoscience*, *5*(6), 410–413. https://doi.org/10.1038/ngeo1465

Toda, S., Stein, R. S., Richards-Dinger, K. B., & Bozkurt, S. B. (2005). Forecasting the evolution of seismicity in southern California: Animations built on earthquake stress transfer. *Journal of Geophysical Research*, *110*, B05S16. https://doi.org/10.1029/2004JB003415

Townend, J., & Zoback, M. D. (2000). How faulting keeps the crust strong. *Geology*, *28*(5), 399–402. https://doi.org/10.1130/0091-7613(2000)28%3C399:HFKTCS%3E2.0.CO;2

Weingarten, M., Ge, S., Godt, J. W., Bekins, B. A., & Rubinstein, J. L. (2015). High-rate injection is associated with the increase in U.S. mid-continent seismicity. *Science*, *348*(6241), 1336–1340. https://doi.org/10.1126/science.aab1345

Wells, D. L., & Coppersmith, K. J. (1994). New empirical relationships among magnitude, rupture length, rupture width, rupture area, and surface displacement. *Bulletin of the Seismological Society of America*, *84*(4), 974–1002.

Yeck, W. L., Hayes, G. P., McNamara, D. E., Rubinstein, J. L., Barnhart, W. D., Earle, P. S., & Benz, H. M. (2017). Oklahoma experiences largest earthquake during ongoing regional wastewater injection hazard mitigation efforts. *Geophysical Research Letters*, *44*, 711–717. https://doi.org/10.1002/2016GL071685

Yeck, W. L., Sheehan, A. F., Benz, H. M., Weingarten, M., & Nakai, J. (2016). Rapid response, monitoring, and mitigation of induced seismicity near Greeley, Colorado. *Seismological Research Letters*, *87*(4), 837–847. https://doi.org/10.1785/0220150275

Yeck, W. L., Weingarten, M., Benz, H. M., McNamara, D. E., Bergman, E. A., Herrmann, R. B., et al. (2016). Far-field pressurization likely caused one of the largest injection induced earthquakes by reactivating a large preexisting basement fault structure. *Geophysical Research Letters*, *43*, 10,198–10,207. https://doi.org/10.1002/2016GL070861

Ziv, A., & Rubin, A. M. (2000). Static stress transfer and earthquake triggering: No lower threshold in sight? *Journal of Geophysical Research: Solid Earth*, *105*, 13,631–13,642. https://doi.org/10.1029/2000JB900081